Numerical Modeling of an Orographically Enhanced Precipitation Event Associated with Tropical Storm Rachel over Taiwan

SEN CHIAO AND YUH-LANG LIN

Department of Marine, Earth and Atmospheric Sciences, North Carolina State University, Raleigh, North Carolina

(Manuscript received 5 September 2001, in final form 9 December 2002)

ABSTRACT

An orographic rainfall event that occurred on 6–7 August 1999 during the passage of Tropical Storm (TS) Rachel over Taiwan is investigated by performing triply nested, nonhydrostatic numerical simulations using the Naval Research Laboratory's (NRL) Coupled Ocean–Atmosphere Mesoscale Prediction System (COAMPS) model. By examining both observational data and numerical model output, it is found that this orographic rainfall event may be separated into three distinct stages. During the first stage (0000–1200 UTC 6 August), TS Rachel was located in the South China Sea and tracked northeastward to Taiwan. Meanwhile, TS Paul was steered by the subtropical high over southwest Japan. During the second stage (1200 UTC 6 August–0000 UTC 7 August), the southwesterly monsoon current as well as the circulation of TS Rachel over southwest Taiwan strengthened and formed a low-level jet (LLJ) with high equivalent potential temperature when TS Rachel moved closer to Taiwan. In comparing the control and sensitivity (without orography) experiments, it was found that the strong LLJ triggered convective systems in the concave region of the southwest Central Mountain Range (CMR), which then produced the first episode of heavy rainfall. The second episode of heavy rainfall, which occurred during the third stage (0000–1800 7 August), was attributed to the modification of TS Rachel's own rainbands by the mountains as well as the strong southwesterly flow impinging on the mountains. The low-level convergence was propagated upstream over the sea, and the impinging flow from southwest Taiwan produced new convective cells. The orographic vertical moisture flux, which is a product of low-level horizontal velocity, mountain steepness, and moisture content, is calculated based on the fine-resolution model output. The regions of maximum moisture flux roughly coincide with the heavy-rainfall regions over the island during this event, while the regions of the general vertical moisture flux coincide with the heavy-rainfall regions over the ocean. Hence, the orographic vertical moisture flux may serve as an index for predicting this type of upslope orographic heavy rainfall. Overall, the model is able to predict the storm track, rainbands, and period of rainfall reasonably well over southern Taiwan, although the maximum rainfall may be slightly overpredicted. Nevertheless, the model results also suggest that a finer-resolution domain or vortex bogusing might be needed for the simulation of precipitation in association with a tropical storm over complex terrain.

1. Introduction

In this study, we consider a heavy orographic rainfall event associated with the passage of a tropical storm over Taiwan. During early August 1999, Tropical Storm Rachel made landfall on the southwestern side of the island. Although the Central Mountain Range (CMR) reduced the strength of this tropical storm when it made landfall, it also provided favorable conditions for the moist airstream to be lifted and to release conditional or convective instabilities. Additionally, the mesoscale forcing by orography on this weather system may also play some important roles in producing heavy rainfall during this event. The operational numerical guidance and forecasts at Taiwan's Central Weather Bureau were not adequate in this case and, thus, did not alert the general public to the potential for heavy rainfall. Obviously, the nature of the orographic modification of this weather system is unclear. The main focus of the present work will be on the mechanisms by which the moist airstreams propagate and behave in relation to the orography as well as to the background synoptic flow in which they are embedded.

Chu and Lin (2000) used the moist Froude number, that is, $F_w = U/N_w h_m$, where U is the basic flow speed near the mountain, N_w is the moist static stability of the incoming airflow, and h_m is the mountain height, to determine the location of orographic rainfall. According to their study, a large F_w (≥ 0.5) does not seem to favor upslope heavy rainfall events. On the other hand, it has been demonstrated by other studies (e.g., Lin 1993; Buzzi et al. 1998) that the majority of orographically induced flash flooding events were associated with a low-level jet (LLJ). In addition, LLJs in the Great Plains of the United States were also found to be important for

Corresponding author address: Prof. Yuh-Lang Lin, Dept. of Marine, Earth and Atmospheric Sciences, North Carolina State University, Box 8208, Raleigh, NC 27695-8208.
E-mail: yl_lin@ncsu.edu

their rapid transport of heat and moisture from the Gulf region into areas of convective storms, which produce heavy rainfall (e.g., Maddox 1983). In this study, we will also examine the role of an LLJ in a real-case simulation.

Lin et al. (2001) proposed nine common ingredients for producing heavy orographic rainfall, which include high precipitation efficiency within the incoming airstream, the presence of a low-level jet, a steep mountain, favorable mountain geometry and confluent flow field, strong synoptically forced vertical motion, high horizontal moisture flow upstream, a large convective system, slow movement of the convective system, and a conditionally or potentially unstable airstream upstream. In addition, a low-level flow with high equivalent potential temperature (θ_e) may induce the potential (convective) instability, which favors the formation of orographic precipitation systems. This type of flow has been observed to exist ahead of fronts or other weather systems, which may serve as a conveyor belt that transports warm and moist air along the upslope side of the terrain (Lin 1993). Therefore, it is very important to understand the various dynamic processes of orographic rainfall. One of our objectives is to examine the common ingredients for heavy orographic rainfall by numerical simulations.

Alpert (1986) has shown that the moisture flux convergence associated with orographic rain enhancement over two-dimensional high mountains could be estimated by assuming that the moisture convergence due to the horizontal wind impinging upon the mountain slope is proportional to the rain enhancement. Sinclair (1994) has shown that precipitation over complex terrain can be reasonably estimated in a first-guess approximation by estimation of the topographically forced vertical motion. Doswell et al. (1998) suggested that substantial moisture flux convergence is needed when rising air is forced orographically. Lin et al. (2001) also suggested that the terrain-induced moisture flux convergence is one of the common ingredients for heavy orographic rainfall and that it may combine with other common ingredients to produce heavy orographic rainfall. Although the results from previous studies provide some guidance in the estimation of heavy orographic rainfall and have addressed the important role that topography plays in generating heavy precipitation, it is still worthwhile to learn how and in what manner the orographic precipitation varies spatially and temporally. In addition to the shortfalls from model resolution and initial conditions, it appears some additional favorable conditions must coexist with those previously mentioned in generating orographic precipitation systems. As indicated in Wu and Kuo (1999), because the rainfall distribution for a typhoon affecting Taiwan is strongly influenced by the orography, the numerical prediction of mesoscale precipitation distribution associated with a typhoon landfalling in Taiwan is a big challenge. It is therefore worthwhile to use a nonhydrostatic model with sufficient horizontal resolution (e.g. grid spacing less than 5 km) to better understand the role that orographic vertical moisture flux plays in heavy rainfall events.

It is one of our objectives to propose a strategy for numerically predicting the orographic rainfall associated with certain weather systems such as frontal systems or landfalling tropical cyclones. A numerical model with more complete atmospheric physics will be used to study the evolution of orographic rainfall induced by Tropical Storm Rachel. Appropriate nested domains with sufficient horizontal resolution to account for the complex topography are used in order to accurately simulate mesoscale orographic phenomena and improve the understanding of dynamical processes of orographic rainfall.

This paper is organized as follows. The description of the atmospheric model is given in section 2. Section 3 discusses the synoptic and mesoscale environmental situations associated with the orographic rainfall event that occurred on 6–7 August 1999 in Taiwan. In section 4, the generation of heavy rainfall is discussed. Some common ingredients associated with the flow and orography will also be examined throughout the entire life cycle of the heavy orographic rainfall event. In section 5, we conclude this study with a discussion based on our interpretation of the simulation results with particular emphasis on application to orographic precipitation forecasting.

2. Description of the model and experiment design

The atmospheric component of the Naval Research Laboratory's (NRL) Coupled Ocean/Atmosphere Mesoscale Prediction System (COAMPS; Hodur 1997) is used in this study. The fully compressible, nonhydrostatic governing equations in the terrain-following vertical coordinate (Gal-Chen and Somerville 1975) are solved by using a second-order finite-difference scheme. A semi-implicit scheme with time-splitting treatment for the acoustic modes enables efficient integration of the fully compressible equations (Klemp and Wilhelmson 1978; Durran and Klemp 1983).

Physical parameterizations include short- and longwave radiation (Harshvardhan et al. 1987). The planetary boundary layer and free-atmospheric turbulent mixing and diffusion are parameterized by using a prognostic equation for the turbulent kinetic energy budget based on the 2.5-level formulation of Therry and Lacarrére (1983). The surface fluxes are computed following Louis's (1979) formulation and the subgrid-scale moist convective processes are parameterized following Kain and Fritsch (1993). The grid-scale evolution of moist processes is explicitly predicted from microphysical budget equations for cloud water, cloud ice, raindrops, snowflakes, and water vapor (Rutledge and Hobbs 1983; Lin et al. 1983). More detailed information on COAMPS can be found in Haack (1996).

A 48-h simulation, starting at 0000 UTC 6 August

1999, utilized the incremental update data assimilation procedure that enabled mesoscale circulations to be retained in the analysis increment fields. The initial fields were created from multivariate optimum interpolation (MVOI) analyses of the surface, upper-air sounding, aircraft, and satellite data that were quality controlled (Barker 1992) and blended with 1° resolution first-guess fields from the U.S. Navy Operational Global Analysis and Prediction System (NOGAPS; Hogan et al. 1991) following Barker (1992). Therefore, the COAMPS prediction system applied in this incremental update methodology mimicked a real-time forecast application. Time-dependent lateral boundary conditions made use of NOGAPS forecast fields (Davies 1976).

The computational domain for the present study was configured on a Lambert conformal projection with three horizontally nested domains encompassing 91 × 101, 151 × 151, and 133 × 133 grid points, respectively. The gridpoint spacings of these computational meshes were 45, 15, and 5 km, respectively. The horizontal area extends from the northwest Pacific, westward to China, and includes Taiwan and parts of western China (Fig. 1a). A total of 30 vertical levels were used, in which 11 levels were distributed in the lowest 2.0 km in order to sufficiently resolve the planetary boundary layer. The model contains the 1-km resolution terrain data that is mapped to the COAMPS model grid resolution to better account for the effects of topography on mesoscale phenomena. The terrain data for the third (i.e., finest) grid mesh of $\Delta x = 5$ km are shown in Fig. 1b. The model topography data are representative of the complex local topographic features, with several mountain peaks to the north and middle of the CMR higher than 3800 m, and a concave geometry located in the southwestern part of Taiwan.

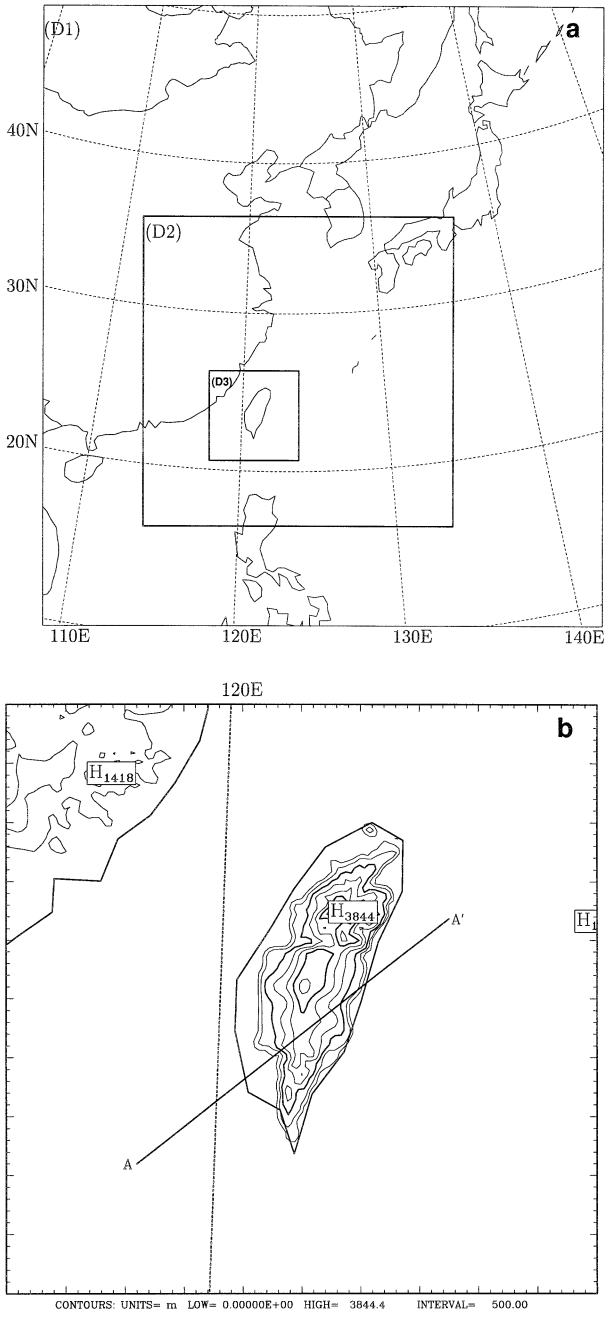

FIG. 1. (a) COAMPS model computational domain. The grid increments for the three nested meshes are 45, 15, and 5 km, respectively. (b) Terrain (every 500 m) used for the 5-km resolution grids. The solid line AA′ represents the orientation of the *x*–*z* cross section in subsequent analyses.

3. Synoptic and mesoscale environments associated with Tropical Storm Rachel (1999)

a. Overview of the synoptic conditions

Tropical Storm (TS) Rachel formed in the monsoon trough of the South China Sea, approximately 260 km southeast of Hong Kong, on 5 August, 1999. The Joint Typhoon Warning Center (JTWC) issued the first warning on TS Rachel at 0900 UTC 6 August. The storm had reached its maximum intensity of 35 kt (~17 m s^{-1}) 3 h later. By 6 August, the surface analysis at 0000 UTC indicated that Tropical Storm Rachel (996 hPa) was located at 21.0°N, 117.9°E in the South China Sea (Fig. 2a). Associated with this tropical storm was a southwesterly wind, which brought moist air in to impinge on the CMR. Meanwhile, TS Paul (990 hPa) was located at 27.9°N, 133.2°E. It had been steered by the subtropical high since early August. At 0000 UTC 7 August, the surface analysis indicated that TS Rachel would move over Taiwan in the next 24 h, and TS Paul had already skimmed the southwest coast of Kyushu Island (Fig. 2b). Figure 3a shows the best tracks of TS Rachel and TS Paul, indicating that TS Rachel tracked northeastward to Taiwan, and made landfall around 0600 UTC 7 August. The finescale (i.e., 5 km) simulation results indicated that TS Rachel filled when it crossed over the CMR (Fig. 3b).

Figure 4 represents the 500-hPa wind and geopoten-

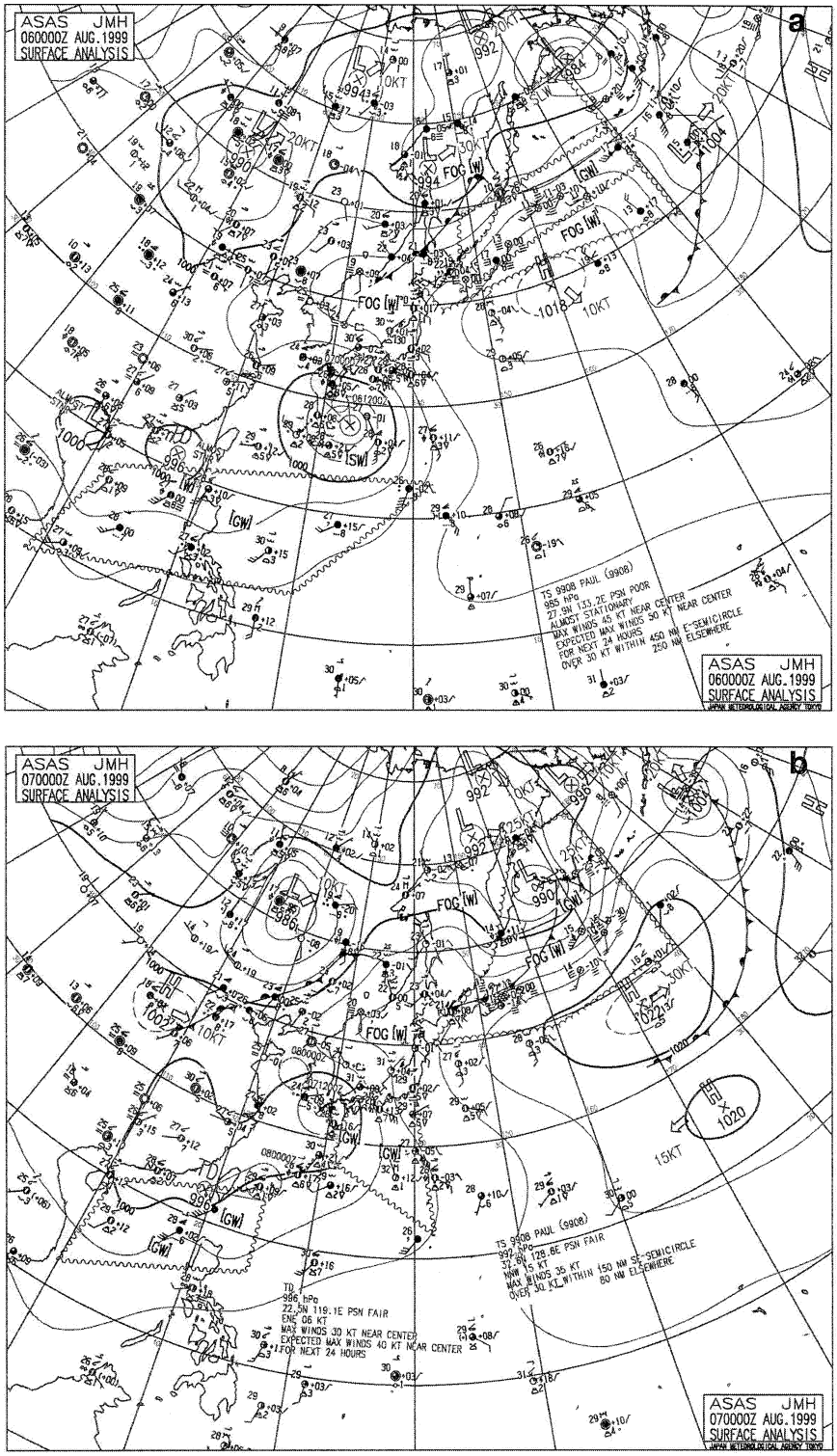

FIG. 2. (a) Surface analysis charts over east Asia valid at 0000 UTC 6 Aug 1999 and (b) surface analysis charts over east Asia valid at 0000 UTC 7 Aug 1999. (From the Japan Meteorological Agency.)

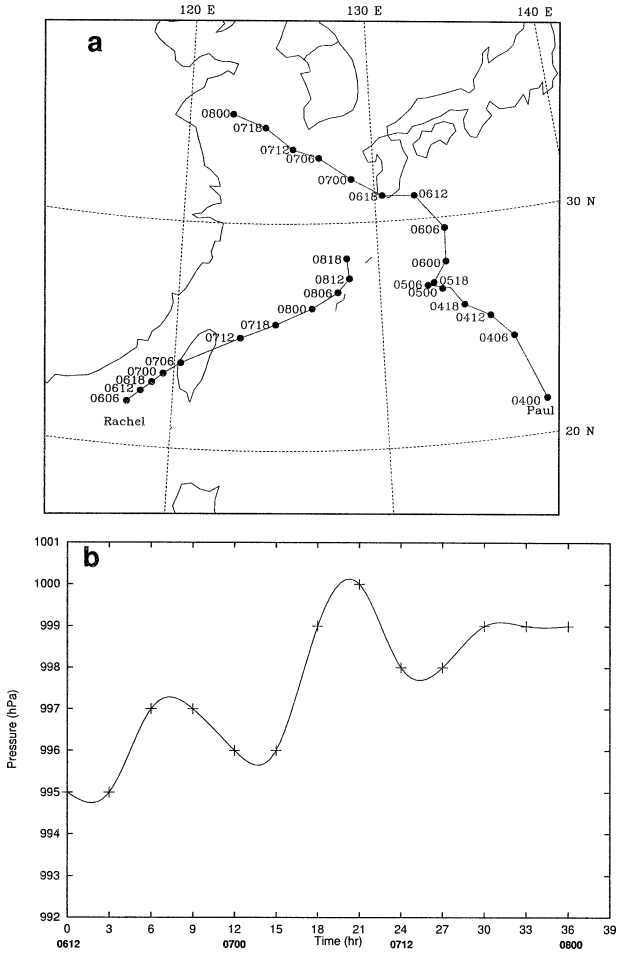

FIG. 3. (a) Best tracks of TS Rachel and TS Paul. (b) The simulated time evolution of TS Rachel's minimum low pressure (hPa). The times for (b) start at 1200 UTC 6 Aug and end at 0000 UTC 8 Aug.

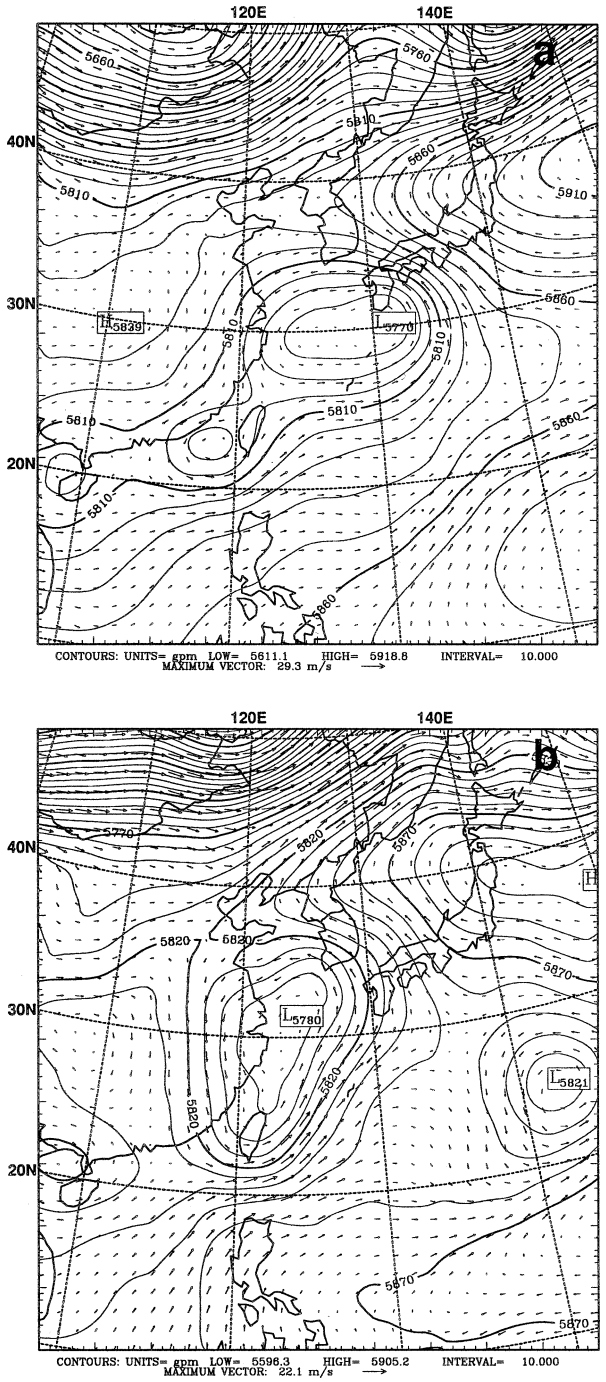

FIG. 4. NOGAPS analysis of 500-hPa geopotential height (m) and wind vector (m s^{-1}) at (a) 1200 UTC 6 Aug and (b) 1200 UTC 7 Aug 1999.

tial height fields, which were analyzed by NOGAPS, valid at 1200 UTC 6 August and 1200 UTC 7 August, respectively. Both TS Rachel and TS Paul were embedded in the monsoon trough at 1200 UTC 6 August (Fig. 4a). At this time the subtropical ridge was located around 38°N and TS Paul moved under the combined influence of the midlevel southwest monsoon flow and the midlevel flow on the southwest periphery of the subtropical high. Tropical Storm Rachel was embedded in the monsoon trough, and steered by the weak flow near the western periphery of the southwesterly monsoon surge. Figure 4b shows the wind and geopotential height fields at 1200 UTC 7 August. Both TS Rachel and TS Paul remained discrete circulations, being embedded in the same large-scale circulation. The same situation was also found at 850 hPa (not shown). As shown in Figs. 4a and 4b, these two tropical storms were influenced by the subtropical high and southwesterly monsoon current. The relative positions of TS Rachel and TS Paul as shown in Figs. 3a and 4 suggest that there might have been some Fujiwhara interaction. However, the binary interactions of the tropical storms are not our main focus in this study. Readers are referred to Fujiwhara (1921), Dong and Neumann (1983), Chang (1983), and Lander (1995) for more detailed discussion about the Fujiwhara effect. Although TS Rachel was

still over the South China Sea, heavy precipitation was recorded over southern Taiwan during this stage.

In general, from 1200 UTC 6 August to 0000 UTC 7 August, the primary importance of TS Paul was to anchor the southwest monsoon well north and east of TS Rachel. This imposed a northeastward steering flow on TS Rachel, allowing it to cross the CMR of Taiwan. In addition, the interaction of the southwest monsoon flow and the southeastward flow on the southwestern periphery of the subtropical high are sufficient to impose the observed cyclonic motion of the two storms. Tropical Storm Rachel brought considerable rainfall to Taiwan in its approach and passage.

b. Mesoscale conditions

At 1800 UTC 6 August, the center of TS Rachel was shown in infrared satellite imagery (Fig. 5a). The radii of TS Rachel are somewhat arbitrary and represent the entire circulation. Imagery also indicates that TS Rachel was embedded in the broad southwesterly flow upstream before landfall. As TS Rachel approached southern Taiwan, the southwesterly flow that impinged on CMR became more apparent. Figure 5b shows the infrared satellite imagery at 0600 UTC 7 August. Although the center of this weak tropical storm was not clearly shown in the satellite imagery at this time, it was located around the southwest coast of Taiwan. The center was covered with a mesoscale precipitation shield, which covered the mountainous terrain of southwest and central Taiwan. A comparison of the evening and morning infrared satellite images shows some dramatic changes in the cloud-top structure. The 1800 UTC image shows that TS Rachel has a relatively symmetric cloud system center. At 0600 UTC, from the satellite image, TS Paul was losing most of its deep convection. It also implied that new strong convection was induced by the CMR during the time TS Rachel made landfall. Subsequently, TS Rachel became disorganized and filled over the CMR.

Since the strong southwesterly flow and the outer circulation of TS Rachel had reached the southern part of Taiwan, the orographic rainfall was observed before TS Rachel made landfall, or between 1200 UTC 6 August and 0000 UTC 7 August. Figure 6a displays the 3-h accumulated precipitation from 1500 to 1800 UTC 6 August. Significant rainfall (~60 mm) had been recorded at the southern peninsula. Apparently, the precipitation was due to the orographic forcing, in which the steep terrain in the southern peninsula of Taiwan affected the impinging flow, rather than from the rainbands of TS Rachel. This is evidenced in the satellite imagery (Fig. 5a), indicating that the rainfall on southern Taiwan during this particular time was not directly associated with Rachel's moist processes. Figure 6b shows the 3-h accumulated precipitation from 1800 to 21 UTC 6 August, and orographic rainfall could still be found along the windward side of southern Taiwan. Notice that due to the movement of TS Rachel, the distribution of the rainfall area had moved farther north. From 2100 UTC 6 August to 0000 UTC 7 August, the accumulated precipitation was found broadly over the southern part of Taiwan (not shown). While the maximum rainfall area was still around the southern tip of Taiwan, the total amount of rainfall had reduced to 40 mm during this time period.

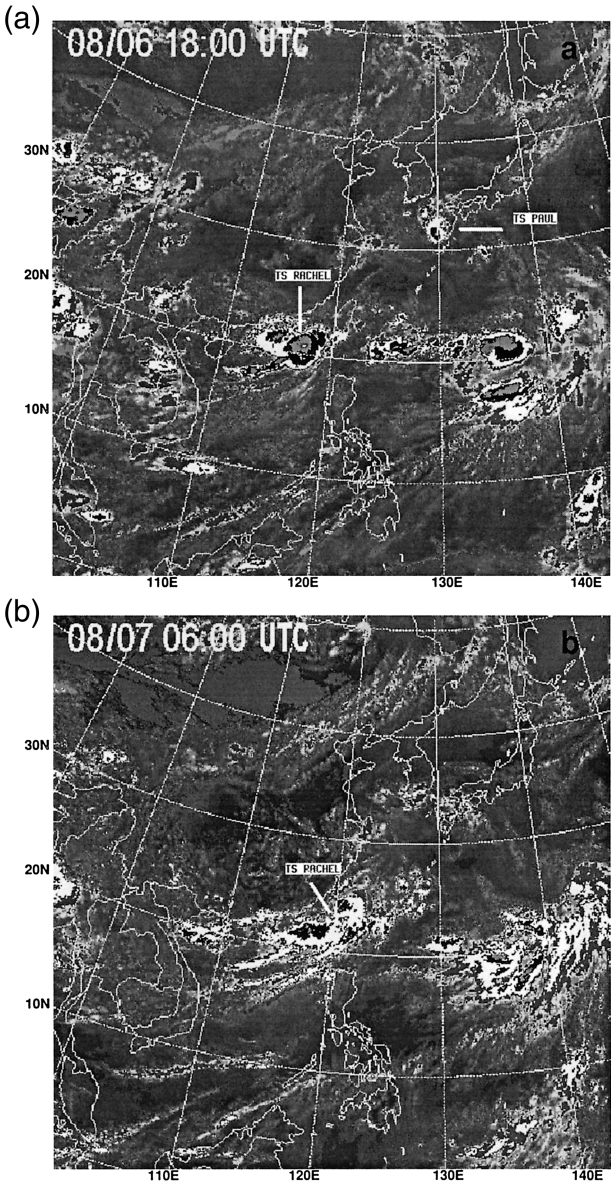

FIG. 5. *GMS-5* visible satellite images at (a) 1800 UTC 6 Aug and (b) 0600 UTC 7 Aug 1999.

Precipitation was assumed to be enhanced when TS Rachel moved inland, where a continuously moist flow was forced to rise over elevated terrain. This was the second rainfall episode that occurred during 0000–0600 UTC 7 August. Figure 6c shows the 3-h accumulated precipitation during TS Rachel's landfall period (0000–

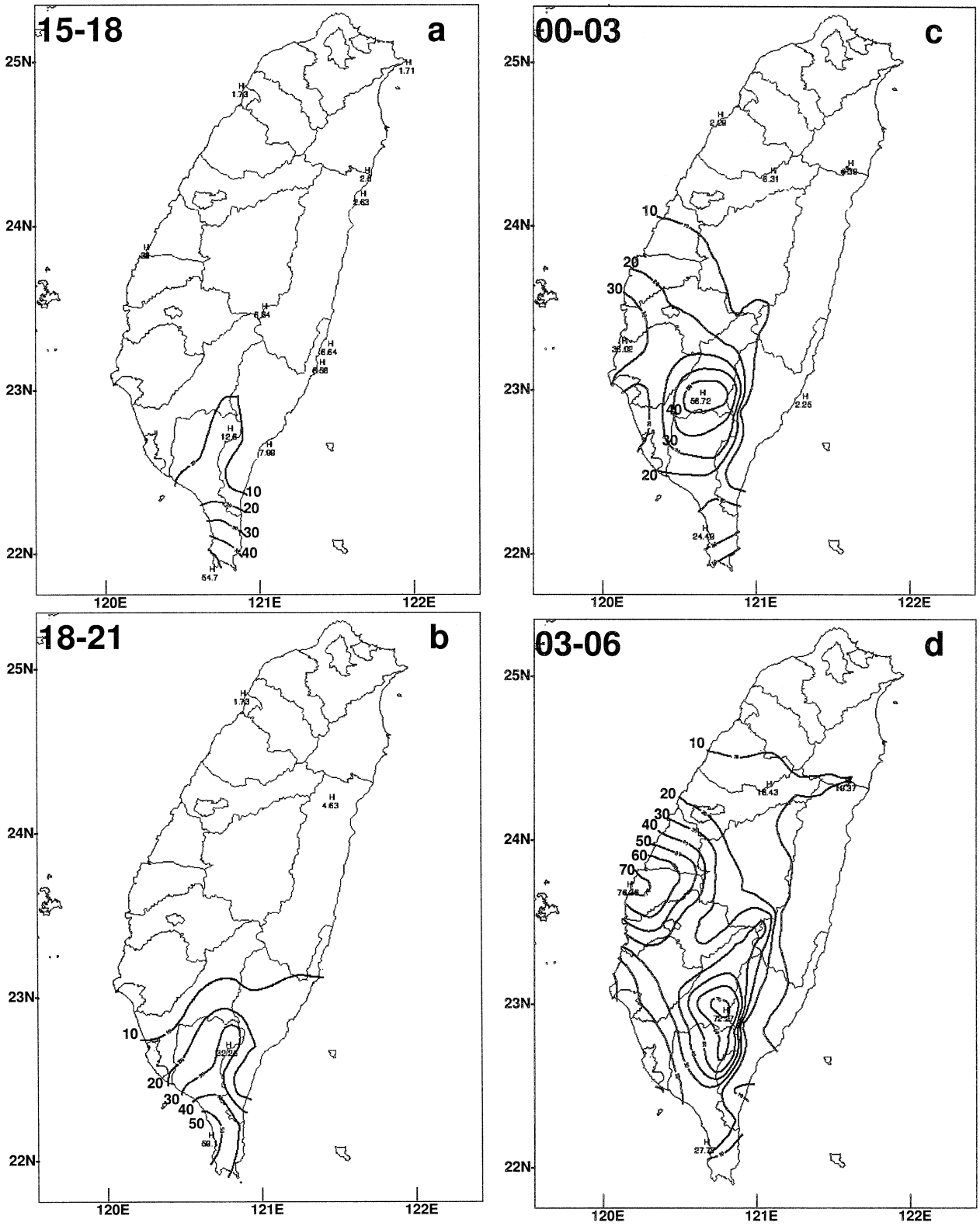

FIG. 6. Analysis of the observed 3-h total accumulated rainfall (mm) over, Taiwan valid at (a) 1500–1800 UTC 6 Aug, (b) 1800–2100 UTC 6 Aug, (c) 0000–0300 UTC 7 Aug, and (d) 0300–0600 UTC 7 Aug 1999.

0300 UTC August 7). Precipitation was found at the slope of a concave area as well as the coastal region of southern Taiwan. More than 50 mm had been recorded within 3 h. The peak amount of the rainfall area was located around Yuh-You (22.59°N, 120.42°E; station height, 1518 m). During 0300–0600 UTC 7 August, TS Rachel gradually filled as it approached Taiwan (as illustrated in Fig. 3b). Figure 6d shows the distribution of the 3-h accumulated precipitation. Apparently, the total precipitation increased while TS Rachel moved toward Taiwan. In addition, the heavy precipitation area was still located around southern Taiwan and the west coast of central Taiwan, while no significant rainfall fell on the east side of the CMR before or during TS Rachel's landfall. It will be shown later that the convection of TS Rachel was enhanced by strong vertical motion induced by the mountains. It is worthwhile to note that during this period when TS Rachel was moving inland, the precipitation could be found not only on the windward slope of the concave area (see Fig. 1b), but also along the coastal area. However, there was no upslope wind over the western coastal area. This implies that some other moist processes were in progress. We hypothesize that these new convective systems along the western coastal area were induced by the vertical moisture flux associated with convergence of the incoming airstream. The evolution of the precipitation distribution is given in the next section.

4. Results of numerical experiments

a. Finescale simulation of orographic rainfall

It is well recognized that increasing model resolution with proper initial conditions for the simulation of orographic rain events will significantly improve the rainfall prediction (e.g., Cacciamani et al. 2000). In other words, high-resolution simulations can offer better insight and understanding of the physical processes and mechanisms of orographic precipitation. For this reason, we shall limit our discussion to only the finescale simulation (5 km), and focus on a comparison between the 5-km resolution simulation results and observations.

As discussed in the previous section, due to the strength of the impinging southwesterly flow during the second stage, heavy orographic rainfall was observed from 1200 UTC 6 August to 0000 UTC 7 August. Figure 7a shows the numerically simulated 3-h accumulated precipitation distribution from 1500 to 18 UTC on 6 August. The results indicated that most of the precipitation was located in southern Taiwan, especially in and around the peninsula area. Some convective cells can be found over the open ocean. Although the amount of simulated precipitation was higher than what the rain gauges actually recorded, the simulated rainfall distribution pattern is relatively consistent with the observed rainfall distribution (Fig. 6a). From 1800 to 2100 UTC 6 August, precipitation was still occurring along the southern peninsula, since the strength of the impinging southwesterly flow increased as TS Rachel approached, and subsequently the rainfall patterns were shifted to the east side of southern Taiwan (Fig. 7b). Compared with the observed results (Fig. 6b), the model results did reproduce the location of rainfall over the southern CMR. The orographic rainfall was still simulated from 2100 to 00 UTC 7 August, as a broad precipitation shield around the peninsula of the southern Taiwan and the rainfall distribution was about the same as 3 h before (not shown). It appears that the mountains played an important role in triggering and redistributing the precipitation, even though TS Rachel had not yet made landfall during this stage.

During 0000–0300 UTC 7 August, most of the simulated precipitation was located in southern Taiwan, especially in the concave region of the CMR (Fig. 7c). Although the simulation was not able to capture the observed local rainfall over the middle of the west coast, the simulated precipitation amount over southern Taiwan (~90 mm) may be somewhat higher than that observed (~60 mm; Fig. 6c). As indicated in the infrared satellite imagery (Fig. 5b), the circulation of TS Rachel was not well organized when it moved closer to the CMR. As shown in Fig. 7d, rainfall could still be found over southern Taiwan from 0300–0600 06 UTC, and some local convective cells were found over the northern and central parts of Taiwan. Compared with observational analysis (Fig. 6d), besides missing the local rainfall over the west coast and overpredicting the rainfall over southern Taiwan, the model roughly captures the pattern of heavy precipitation over southern Taiwan. In summary, from 0000 to 0600 UTC 7 August, the simulation results demonstrated that the heavy rainfall area was found along the slopes of the concave area as well as the southern peninsula of Taiwan. Although the model did not adequately simulate the local rainfall over the middle west coast, it was able to simulate the location of the heavy precipitation region over southern Taiwan during this period, and the total amount of rainfall was overpredicted by about 70 mm (~30%).

Besides the control simulation discussed above, in order to isolate the role of orography in this heavy precipitation event, we performed a sensitivity simulation without orography. Figure 8a shows the 3-h accumulated rainfall distribution from 1500 to 1800 UTC 6 August with heavy rain located around southern and southeastern Taiwan. From 1800 to 2100 UTC 6 August, a large portion of the rain was over the ocean to the southeast of Taiwan (Fig. 8b). During 0000–0300 UTC 7 August (Fig. 8c), simulated precipitation was over southern Taiwan, with the maximum rainfall located over the ocean. Three hours later, heavy rainfall still could be found over southern Taiwan (Fig. 8d). However, as TS Rachel moved over the ocean, heavy rainfall was mainly associated with the southwesterly monsoon during this period.

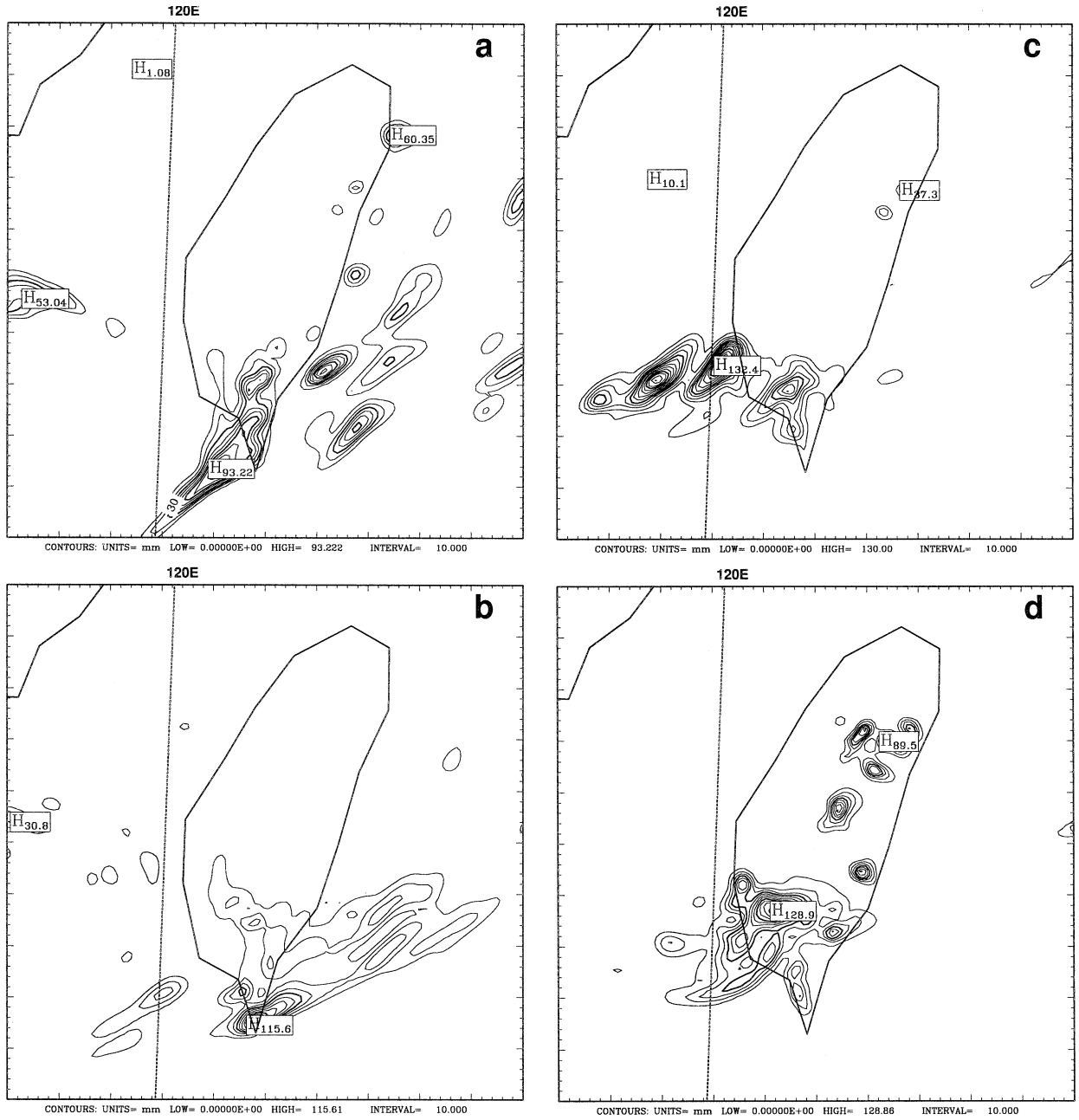

FIG. 7. The 5-km-resolution grid forecast 3-h total accumulated rainfall (mm) over Taiwan valid at (a) 1500–1800 6 Aug, (b) 1800–2100 UTC 6 Aug, (c) 0000–0300 UTC 7 Aug, and (d) 0300–0600 7 Aug 1999.

Comparing the control simulation (Fig. 7) with the sensitivity simulation (Fig. 8), the similarity of the results illustrated in Figs. 7a and 8a suggests that the rainfall amounts and distribution were more a result of the large-scale circulation than of the orography. The differences between Figs. 7b and 8b do suggest that the orography near the southern end of Taiwan may have had some influence in the 1800–2100 UTC time frame. In Figs. 7c and 8c, the results indicate that rainfall was more abundant over Taiwan in the experiment without topography. It is clear that the presence of the topography changed the distribution of TS Rachel's precipitation significantly during the landfall period. In addition, the simulation results indicate that the rainfall patterns seemed to initially start at the slope of the CMR and subsequently propagate to the coast. In other words, the complex topography could induce convection by convergence and organize the localized convective cells. Nevertheless, some other conditions for inducing heavy orographic rainfall must have also been present, in order

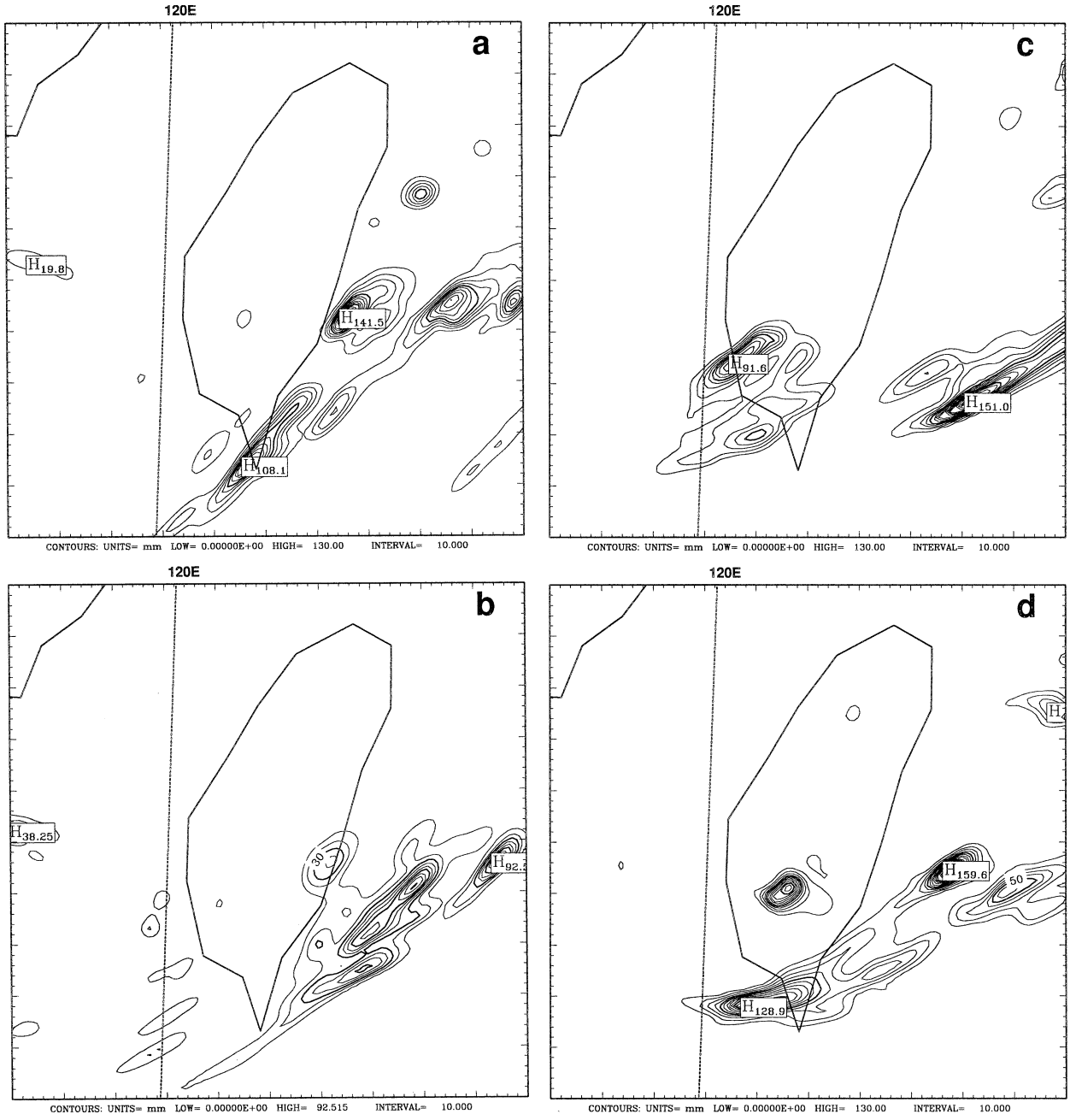

FIG. 8. Same as in Fig. 7 but without orography.

to produce heavy orographic rainfall. We will discuss these conditions in the following section.

b. Some common ingredients for orographic rainfall

In this section we will examine some of the common ingredients that have been proposed by Lin et al. (2001) to explain heavy orographic rainfall for this particular event. The role of a steep mountain as well as favorable mountain geometry will be examined by using the fine-scale simulation results. In addition, the strong southwesterly low-level jet, the presence of a high moisture flow upstream, and a conditionally or potentially unstable upstream airflow will also be discussed.

As discussed in the previous section, the COAMPS model did reasonably well in predicting the distribution of heavy rainfall over the southern CMR during different time periods. After comparing the control simulation and the sensitivity simulation (without orography), it is clear that the steep mountain is an important ingredient

in this case. In particular, it has an approximated steepness value of 0.033 in southern CMR [i.e., h_m/L_x, where h_m (~3 km) is the average mountain height, and L_x (~90 km) is the width of southern Taiwan). As indicated in Fig. 1b, the concave geometry of the CMR is located around 22.8°N, 120.5°E, where the most significant precipitation was observed to occur. As suggested in Lin et al. (2001), the mountain concave geometry and LLJ will give a large value of $\boldsymbol{V}_H \cdot \nabla h$, which then results in heavy precipitation in the concave area. Similar phenomena have also been observed in the Lago Maggiore region over the southern Alps (e.g., Schneidereit and Schär 2000). Orographic rainfall over southern Alpine slopes often starts from the Lago Maggiore region when a moist LLJ flows from the Mediterranean. Another clear example of orographic rainfall enhancement produced by the interaction of the Mediterranean LLJ with the concave geometry occurs in the Valencia region in eastern Spain (see Romero et al. 2000).

Figure 9 shows the horizontal wind vectors and velocities at 850 hPa during the orographic rainfall period. The southwesterly flow dominated the flow field at 2100 UTC 6 August (Fig. 9a) when the direction of impinging wind was nearly perpendicular to the southern part of the CMR. The strong low-level wind (~18 m s^{-1}) was located around the southern peninsula of Taiwan. The upward motion also existed over the foothills of the CMR, and as a result, heavy orographic precipitation was also recorded there. Three hours later, as TS Rachel moved much closer to southern Taiwan, the wind speed at the concave region was enhanced by the combination of the southwesterly monsoon and the outer circulation component of TS Rachel, which served as a low-level jet (Fig. 9b). The upward motion cells were found along the foothills of the southern CMR and over the open ocean. These strong upward motion cells illustrated orographically induced vertical motion as well as the vertical motion associated with TS Rachel, which were consistent with the change of convection from the satellite imagery (Fig. 5b). Figure 9c shows the wind field at 0300 UTC 7 August. Since TS Rachel moved closer to Taiwan at this time, a strong continuous flow coming from the southwest with wind speeds in excess of 15 m s^{-1} located on the lee side of the CMR was produced. The upward vertical velocity field along the coast was oriented in the southwest–northeast direction as TS Rachel continued its northeastward track. At the same time, there was upward motion over northern Taiwan. At 0600 UTC 7 August (Fig. 9d), the region of strong upward motion was well organized in southern Taiwan as TS Rachel moved inland, and the rainfall over southern Taiwan peaked. These upward motions also suggest that grid-explicit convection was produced in the model (e.g., Kain and Fritsch 1998).

Convergence of the flow also formed along the coastline of southwest Taiwan when TS Rachel moved closer to the island. At 0300 UTC 7 August, a convergence zone formed in the concave region where the most significant rainfall was observed. The offshore divergence was associated with the winds redirected by the concave regions (not shown). The area of strong upward motion at 850 hPa (Fig. 9) was correlated with zones of near-surface horizontal wind convergence. In contrast, the horizontal wind field and upward motion at 850 hPa in the sensitivity experiment without orography suggested that TS Rachel moved faster and made landfall at 0300 UTC 7 August (Fig. 10a). Three hours later, TS Rachel had moved to the ocean (Fig. 10b). Some convective cells were embedded in Rachel's circulation as well as in southwesterly flow when TS Rachel was moving over Taiwan. In comparing the results of the control and sensitivity experiments, while the large-scale circulation had some contribution to the rainfall, it is evident that the increased near-surface convergence and upward motion over the concave region of southwestern Taiwan played a role in intensifying the precipitation of TS Rachel as it made landfall (cf. Figs. 7 and 8). In other words, the favorable mountain geometry (i.e., concave area) is another ingredient in enhancing orographic rainfall.

In order to identify the flow-over or flow-around (and blocking) regime of the LLJ impinging on southern Taiwan, we have also calculated the moist Froude number. The F_w upstream of the concave region for this case is about 0.34 (U = 10.0 m s^{-1}, N_w = 0.0098 s^{-1}, h_m = 3000 m), which demonstrated the impinging flow was blocked by the CMR. This flow condition may also be identified as the regime with upstream-propagating convective systems (e.g., Chu and Lin 2000; Chen and Lin 2001). Because of the blocking effects of the southern CMR, the southwesterly winds were split into two components. As indicated in Figs. 9c and 9d, the southwesterly flow on the windward side was significantly redirected northwest into the concave region, while the other component of the impinging southwesterly flow moved around the southern tip of Taiwan. Strong upward motions were simulated over the foothills of the CMR throughout the entire period of heavy orographic rainfall (Fig. 9). Apparently, the blocking effects of the CMR would enhance the vertical motion while TS Rachel moved inland. Comparing the simulated rainfall distributions (Fig. 7) with the wind fields (Fig. 9), it appears that the orographic rainfall was affected by the strong southwesterly LLJ and the convergence near the concave region. Thus, we can conclude that the strong southwesterly low-level jet is another ingredient for producing heavy orographic rainfall.

During the second stage (1200 UTC 6 August–0000 UTC 7 August), the impinging southwesterly flow was very moist since it came from the ocean. The θ_e distributions at 850 hPa at 2100 UTC 6 August and 0300 UTC 7 August (Figs. 11a and 11b) indicate that the impinging southwesterly flow was very moist since southern Taiwan was covered with high-θ_e ($\geq$335 K) flow. The orographic rain started to occur when this tongue of moist air moved toward the southwestern

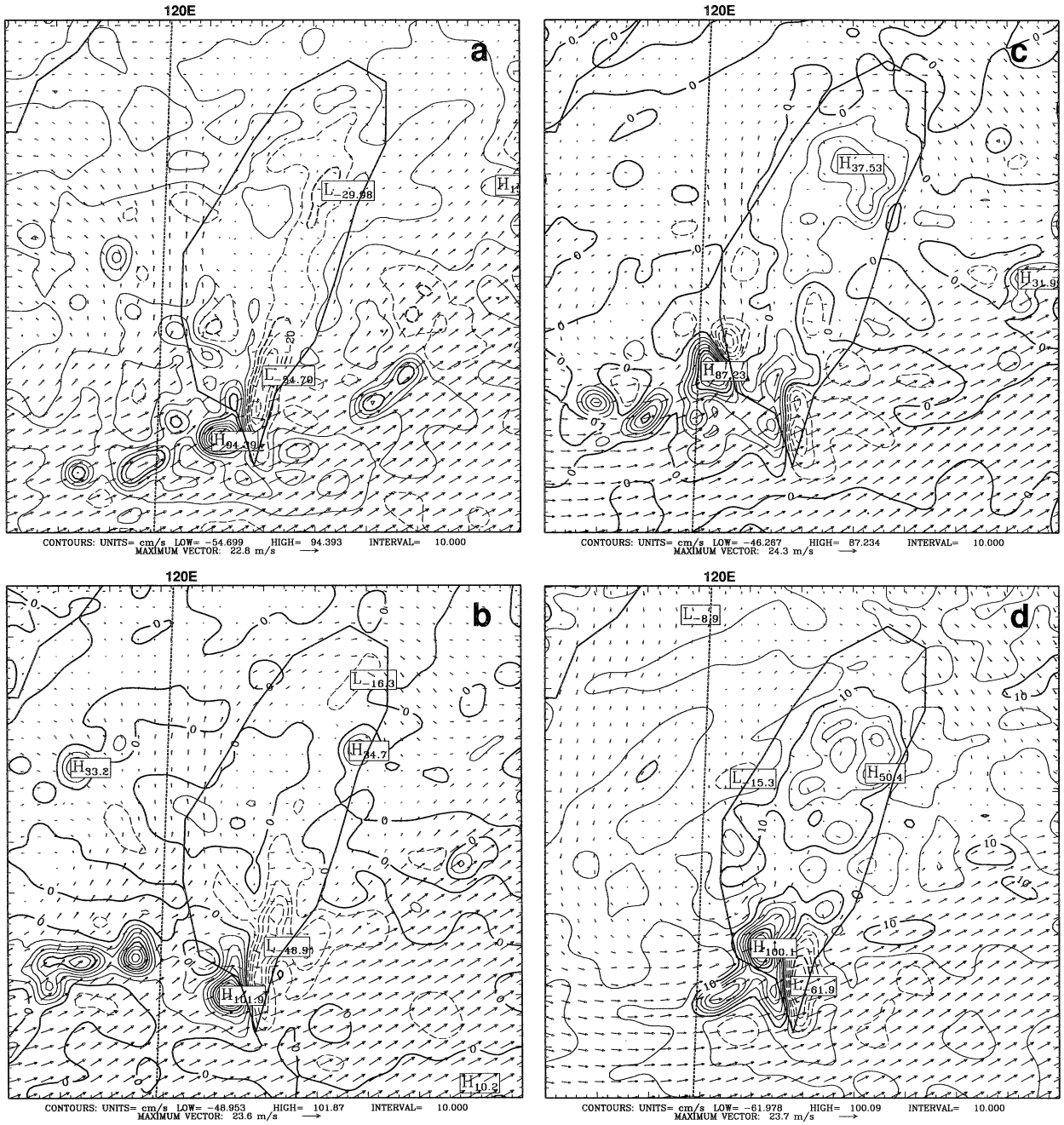

FIG. 9. The simulated 850-hPa wind fields and vertical velocity (every 10 cm s^{-1}) for 5-km-resolution grid valid at (a) 2100 UTC 6 Aug, (b) 0000 UTC 7 Aug, (c) 0300 UTC 7 Aug, and (d) 0600 UTC 7 Aug 1999.

CMR (as illustrated in Fig. 6b). When TS Rachel moved closer to the island, a more significant change of θ_e could be found in the concave region and southern CMR, which was collocated with the heavy rainfall area during that time (Fig. 11b). An area of high θ_e was also found in northeastern Taiwan (Fig. 11b). However, the impinging flow barely existed over northeastern Taiwan and the precipitation was not as heavy as that in southwestern Taiwan. The results suggest that the high moisture airstream is one of the ingredients for producing heavy orographic rainfall.

In order to understand the generation mechanisms of orographic rainfall associated with this event, we use the fine-resolution data generated by the model to examine the orographic precipitation efficiency formula proposed by Lin et al. (2001). Based on their Eq. (8), the total precipitation produced (P) may be estimated by

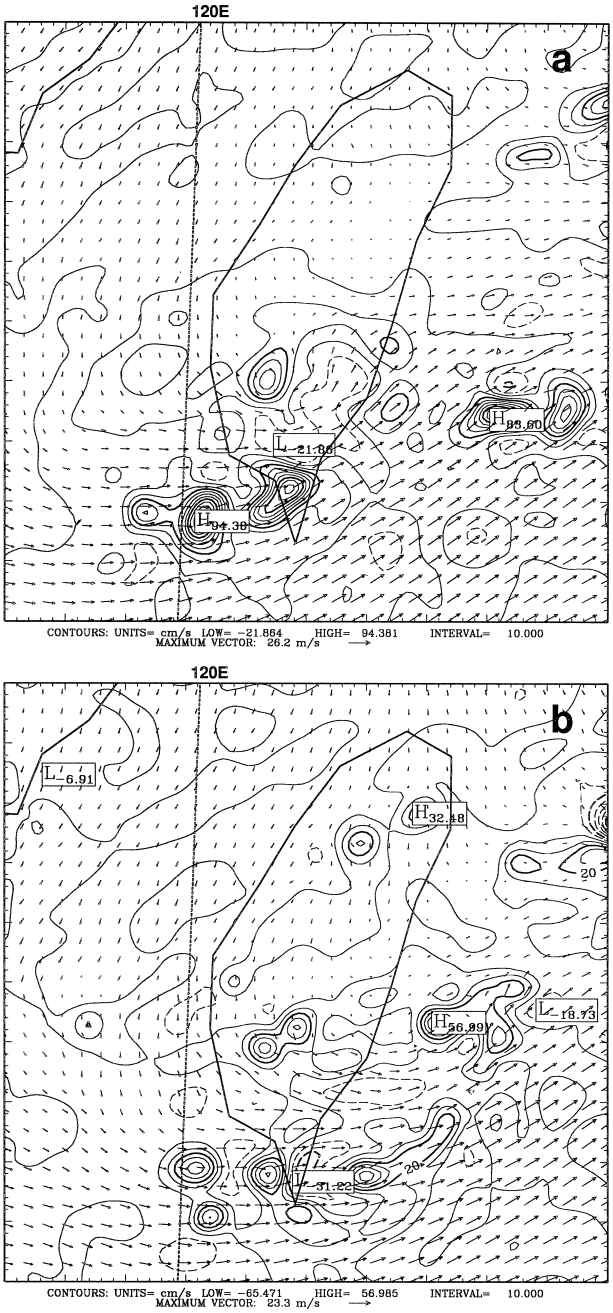

FIG. 10. The 850-hPa wind field and vertical velocity (every 10 cm s^{-1}) for 5-km-resolution grid simulation without orography valid at (a) 0300 and (b) 0600 UTC 7 Aug 1999.

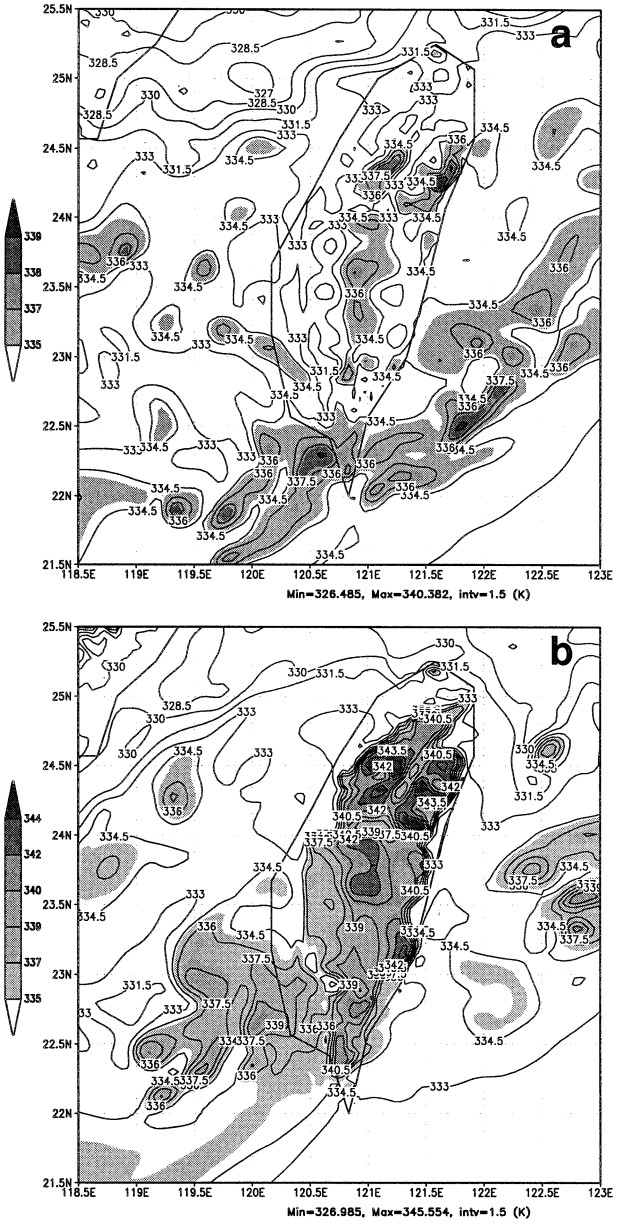

FIG. 11. The simulated equivalent potential temperatures (θ_e) at 850 hPa at (a) 2100 UTC 6 Aug and (b) 0300 UTC 7 Aug 1999. Areas with θ_e greater than 335 K are shaded.

$$P = \frac{\rho}{\rho_w} E(\mathbf{V}_H \cdot \nabla h + w_s)\frac{qL_s}{c_s}, \qquad (1)$$

where $\mathbf{V}_H \cdot \nabla h$ is directly related to the orographically induced vertical motion (Doswell et al. 1998; Lin et al. 2001), w_s is the synoptically forced vertical motion, q is the mixing ratio, ρ and ρ_w are the air density ($\sim$1 kg m^{-3}) and water density ($\sim$1000 kg m^{-3}), c_s is the propagation speed of the convective system, and L_s is the horizontal scale of the convective system. The precipitation efficiency (E) is defined as the ratio of the precipitated water mass to the mass of water vapor inflow (Fankhauser 1988; Doswell et al. 1996). A value for E is not easy to calculate or estimate since it is far more sensitive to the parameterization of cloud microphysics, and the values are ambiguous due to repeated ascent and descent at the convective scale. Both L_s and c_s may be estimated; however, they are too sensitive to be taken into account in Eq. (1). Therefore, the precipitation pro-

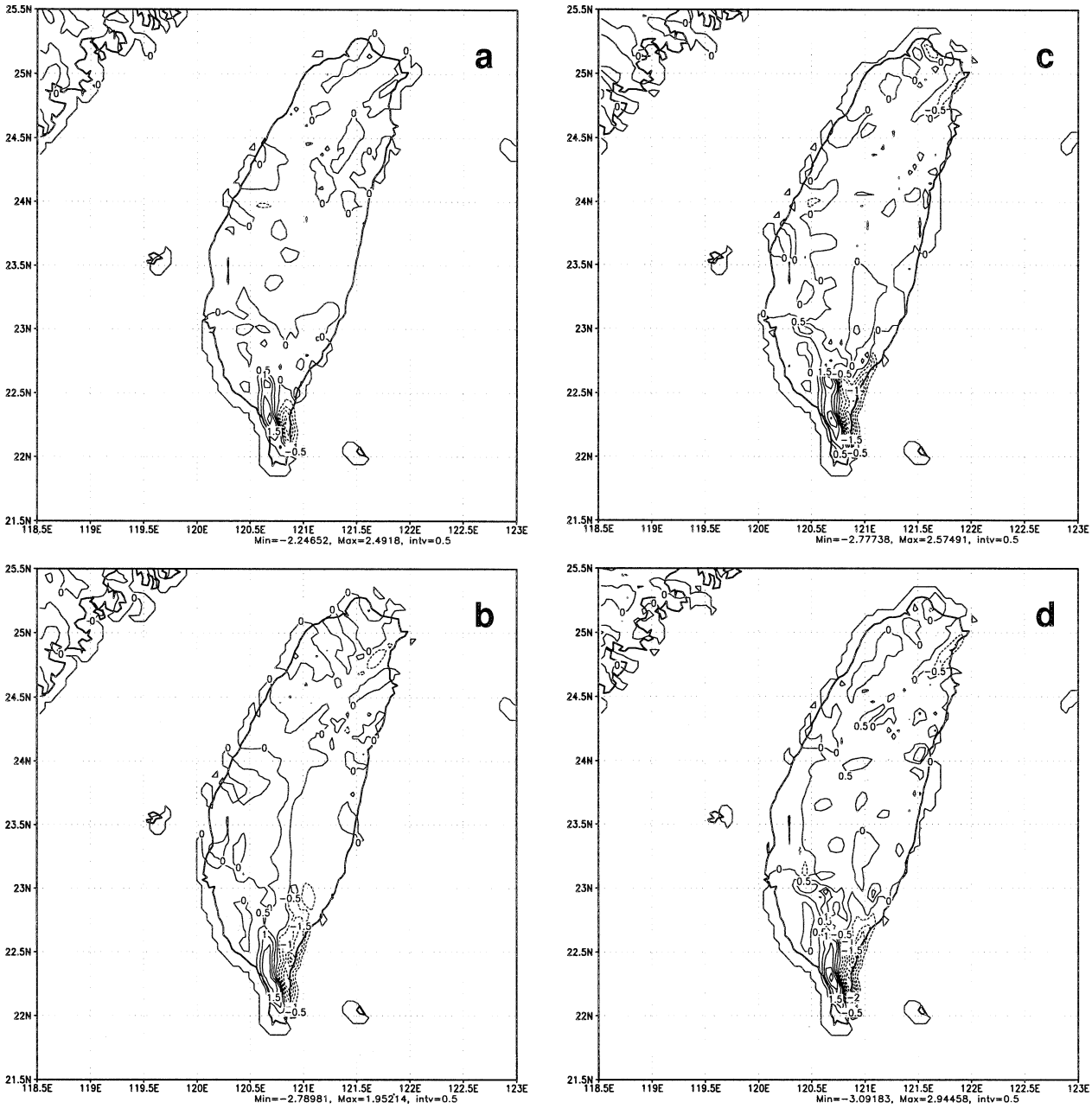

FIG. 12. Topographically induced vertical moisture flux (g kg^{-1} m s^{-1}) at 850 hPa at (a) 1800 UTC 6 Aug, (b) 2100 UTC 6 Aug, (c) 0300 UTC 7 Aug, and (d) 0600 UTC 7 Aug 1999.

duced (P) is roughly proportional to orographically induced vertical motion and synoptically induced vertical motion multiplied by the mixing ratio. We will calculate these two terms individually for this particular case. Although the synoptically forced vertical motion may not be significant in our particular case, the vertical moisture flux associated with it could contribute to the precipitation when the convective system is over a flat area such as the open ocean.

The evolution of the orographically induced moisture flux, that is, $(\mathbf{V}_H \cdot \nabla h)q$ at 850 hPa, is shown in Figs. 12a–d for 1800 and 21 UTC on 6 August, and 0300 and 0600 UTC on 7 August. As mentioned in previous sections, these four times represent the heavy precipitation period induced by orographic effects during the landfall of TS Rachel. Note that $\boldsymbol{V}$ and q vary strongly in time and space, which in turn, causes the vertical moisture flux to vary strongly, also. Therefore, we chose the 850-hPa level to calculate the orographically induced moisture flux, since the

850-hPa level to calculate the orographically induced moisture flux, since the 850-hPa level is less affected by boundary layer processes.

When the southwesterly flow impinges on the mountains, the vertical moisture flux is positive (negative) on the windward (lee) side (Fig. 12a). At 2100 UTC 6 August (Fig. 12b), the high positive value of this vertical moisture flux was still located in southern Taiwan. It can be seen that high vertical moisture flux regions were located along the southwest coast of the island. This result is consistent with the observed (Figs. 6a and 6b) and simulated (Figs. 7a and 7b) heavy orographic rainfall areas. When TS Rachel moved closer to Taiwan, the impinging flow tended to be shifted by the concave region of the CMR. Hence, the terrain-induced vertical moisture flux was more vigorous in southern Taiwan at 0300 UTC 7 August (Fig. 12c). This result also suggests that the precipitation over the southern coast of Taiwan was induced by the vertical moisture flux that was associated with flow convergence. The same situation can be found at 0600 UTC 7 August (Fig. 12d). As indicated in both the observations (Fig. 6d) and the simulations (Fig. 7d), the high precipitation regions were located on the slope of the southern CMR during that time.

Figure 13a shows the vertical moisture flux by using model-predicted vertical motion multiplied by the mixing ratio (wq) at 0300 UTC 7 August at 850 hPa. Compared with Fig. 12c, the general vertical moisture flux did represent that portion of the precipitation over the ocean, as can be seen from the high values of moisture flux located along the coast of Taiwan. Similar results can also be found at 0600 UTC 7 August (Fig. 13b). At this time, large positive values of general vertical moisture flux were located in southern Taiwan with a narrow band that stretched in from the ocean and that is associated with a rainband of TS Rachel. Based on this study, we may conclude that the positive area of orographically induced vertical moisture flux could be used to help forecast areas of potential heavy rainfall over the windward mountain area. The general vertical moisture flux (wq) can predict rainfall over a flat surface, which is not predicted by the orographically induced moisture flux. The orographic vertical moisture flux proposed by Lin et al. (2001) can provide weather forecasters with additional information for forecasting heavy orographic rainfall.

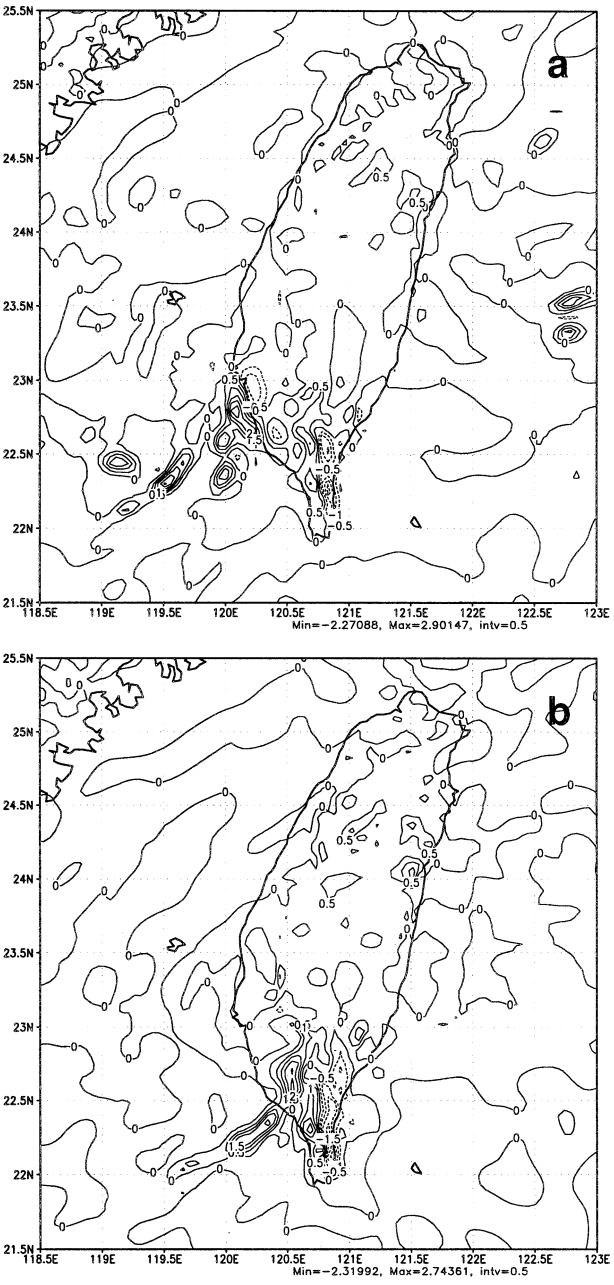

FIG. 13. Total vertical moisture flux (g kg^{-1} m s^{-1}) at 850 hPa at (a) 0300 UTC and (b) 0600 UTC 7 Aug 1999.

Another important process is the triggering of potential instability by the orography. The decrease of θ_e with height implies the possible existence of a potentially unstable layer. The high-θ_e flow has been observed to exist ahead of a front or other weather systems, which may serve as a conveyor belt that transports warm and moist air to the upslope (e.g., Harrold 1973; Lin 1993). The model sounding near the slopes of southern Taiwan (22.6°N, 120.3°E) at 1200 UTC 6 August (Fig. 14a) indicated the lifting condensation layer (LCL) was 0.4 km and the level of free convection (LFC) was lower than 1.0 km. The convective available potential energy (CAPE) was about 818 J kg^{-1} during this time. It appears that the impinging LLJ ($\sim$10 m s^{-1}) in terms of orographic lifting should be able to lift air up to the LFC and produce heavy rainfall. In fact, the depth ($\Delta\eta$) due to orographic lifting can be roughly estimated by assuming $\Delta\eta = w\Delta t$, where $w \approx U(\partial h/\partial x)$. If $U \approx 10$ m s^{-1}, and $\partial h/\partial x \approx 0.033$, the impinging air will be lifted up to LFC after 1 h. At 0000 UTC 7 August, as

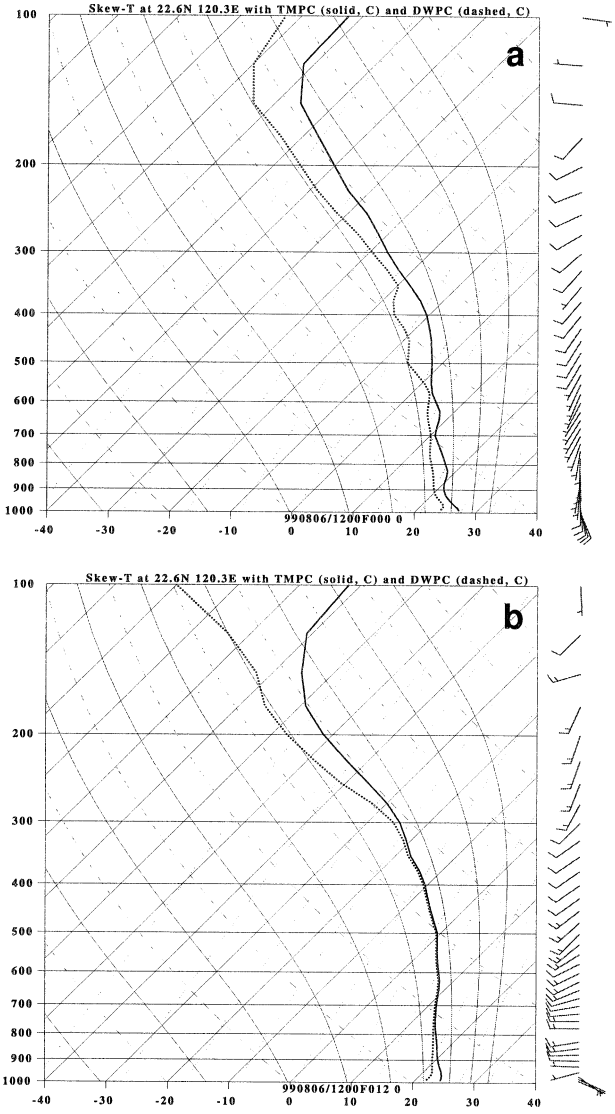

FIG. 14. Skew *T*–log*p* charts from model, located at 22.6°N 120.3°E, at (a) 1200 UTC 6 Aug and (b) 0000 UTC 7 Aug 1999.

TS Rachel moved closer to southern Taiwan, the model sounding becomes almost completely saturated (Fig. 14b). It suggests that latent heat has been released, and CAPE has been consumed and heavy rainfall has been produced. Notice that the sounding at 1200 UTC 6 August (Fig. 14a) indicates that the low-level flow is potentially unstable since $\partial\theta_e/\partial z < 0$.

In order to gain further insight into the potential instability during the heavy orographic rain associated with TS Rachel's landfall, we analyzed the vertical cross section of θ_e from southwest (21.8N, 119.5E) to northeast (24.0N, 122.3E) (see Fig. 1b). The θ_e and cloud water (q_c) on the vertical cross section through the concave region (Fig. 15) indicate intense updrafts and heavy orographic rainfall, which occurred when TS Rachel moved inland. Figure 15a indicates that the potentially unstable layer ($\partial\theta_e/\partial z < 0$) existed upstream of the CMR, and that the regions of high q_c formed upstream and over the top of the mountain, which indicates that convection was forced by orographic blocking at about 2100 UTC 6 August. At 0000 UTC 7 August (Fig. 15b), the θ_e and q_c fields indicate that the moist convection formed upstream of CMR. Additionally, density currents were formed on the upslope of the CMR caused by the evaporatively cooled air (low equivalent potential temperature). In fact, the density currents can be treated as outflow boundaries, which were produced by the convective cold pools (Fig. 15b).

At 0300 UTC 7 August, when TS Rachel moved closer to southern Taiwan (Fig. 15c), a strong enhancement of the θ_e contrast in the lower troposphere existed upstream of the CMR. This contrast of θ_e is associated with the impinging southwesterly flow and Rachel's outer circulation. As a result, two strong potentially unstable layers existed upstream of the CMR (Fig. 15c). Three hours later (Fig. 15d), when TS Rachel made landfall, the θ_e cross section indicates a deep potentially unstable layer over the southwest slope of the CMR. During 0000–0600 UTC 7 August (Figs. 15c and 15d), new convection formed upstream from southern Taiwan. Apparently, the outflow boundaries forced the low-level convergence to propagate upstream over the ocean, and the impinging flow from the southwest triggered new convection.

Figure 16 presents the vertical velocity on cross section AA′, which helps identify the depth and intensity of the updraft rooted over the sloping orography. Specifically, Fig. 16a shows that a strong and deep updraft occurred upstream and upslope of the CMR at 0300 UTC 7 August. It is clear that the orographically induced upward motion occurred as flow impinged on the mountains, while the upstream updraft was part of the circulation of TS Rachel. Three hours later (Fig. 16b), when TS Rachel moved over Taiwan, intense and deep vertical motion occurred over the mountains. It appears that the potentially unstable layer over the ocean was due to the vertical motion embedded in the circulation of TS Rachel, and the potentially unstable layer in mountainous areas was caused by the impinging LLJ associated with orographically induced vertical motion. In addition, these results may help to explain the changes that were found in the cloud-top structure in satellite imagery (Fig. 5b). The potentially unstable regions were collocated with those of the heavy rainfall (Figs. 7c and 7d) as well as the high values of vertical moisture fluxes (Figs. 12 and 13). The location of heavy precipitation was also collocated with the strongly unstable regions. As shown in Fig. 15, some unstable layers existed near the surface both on the windward side and on the lee side. However, no significant rainfall was predicted over the lee side, due to the fact that potential instability could not be released under the conditions of air descent induced by the orography. We conclude that the upward motion induced by the orography and TS Rachel was

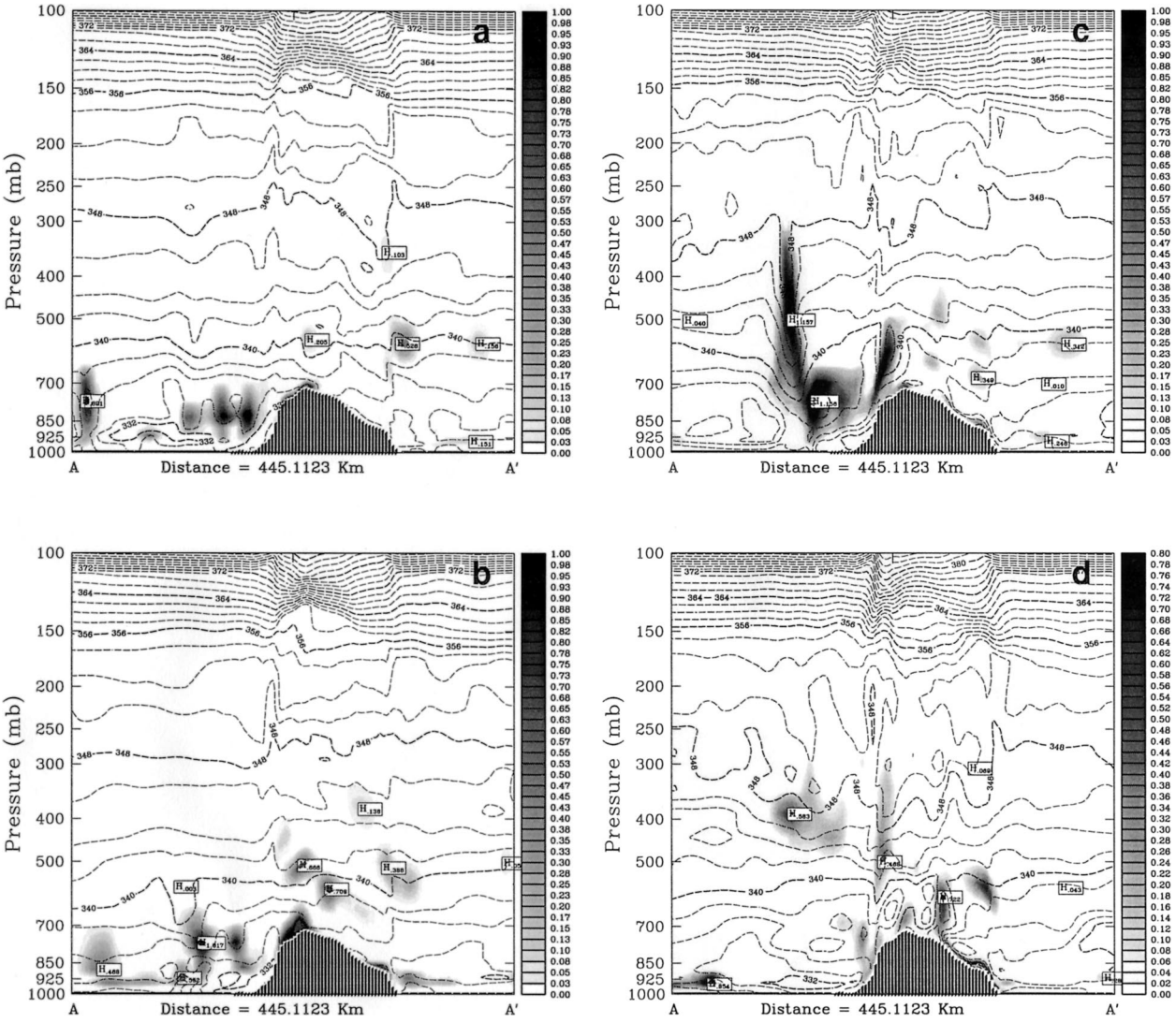

FIG. 15. The x–z cross section of equivalent potential temperature (θ_e, every 2 K) and cloud water (q_c) from 21.8°N, 119.5°E to 24.0°N, 122.3°E (SW → NE) valid at (a) 2100 UTC 6 Aug, (b) 0000 UTC 7 Aug, (c) 0300 UTC 7 Aug, and (d) 0600 UTC 7 Aug 1999. The cross section AA′ is depicted in Fig. 1b. Areas with q_c greater than 0.02 g kg^{-1} are shaded.

able to release the potential instability, which could trigger the strong convection, and produce orographic precipitation.

5. Discussion and conclusions

In this study, numerical experiments were performed to investigate the observed synoptic and mesoscale environments and examine some common ingredients for orographic rain when Tropical Storm Rachel passed over Taiwan. The numerical experiments were conducted using a coupled ocean–atmosphere numerical weather prediction model (COAMPS). Based on a recent study of some common ingredients for orographic rainfall (Lin et al. 2001), we have investigated the evolution of heavy orographic rain to better understand the mechanisms responsible for orographic precipitation.

It was shown that this landfalling tropical storm event could be divided into three distinct stages. From 0000 to 1200 UTC 6 August, TS Rachel was embedded in the monsoon trough of the South China Sea, and moved northeastward toward Taiwan. Meanwhile TS Paul was steered by the subtropical high to the northwest. During the second stage, from 1200 UTC 6 August to 0000 UTC 7 August, the steering flow in the midtroposphere accompanying the subtropical high and the southwesterly monsoon current caused the midtropospheric circulation of TS Paul and TS Rachel to interact with each other, which resulted in counterclockwise rotation of these two storms. In the final stage (0000–1800 UTC 7 August), orographic

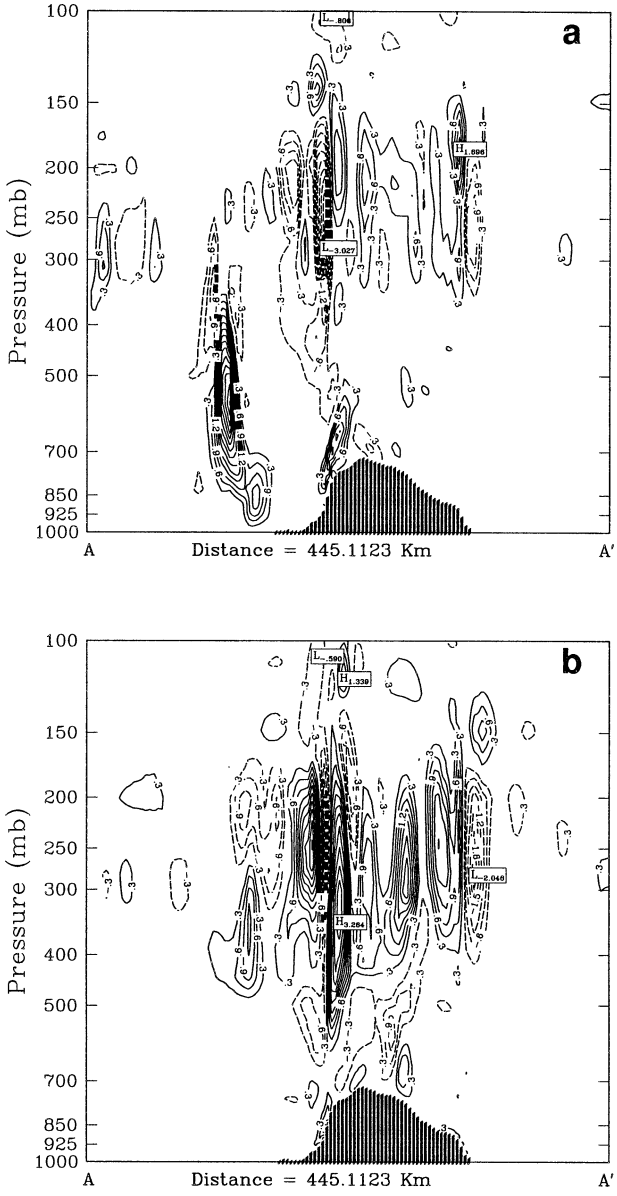

FIG. 16. The x–z cross section of vertical velocity (every 0.3 m s^{-1}) from 21.8°N, 119.5°E to 24.0°N, 122.3°E (SW → NE) valid at (a) 0300 and (b) 0600 UTC 7 Aug 1999. The cross section AA′ is depicted in Fig. 1b.

rainfall was triggered by the continuous strong southwesterly low-level jet impinging on the Central Mountain Range (CMR) of Taiwan. This strong low-level jet was a combination of TS Rachel's direct circulation and the southwesterly monsoon.

During the second stage, the impinging southwesterly flow strengthened and formed a low-level jet (LLJ) with high θ_e due to the approach of TS Rachel toward Taiwan. The heavy precipitation was caused mainly by orographic lifting. Heavy rainfall was still observed between 0000 and 0600 UTC 7 August while TS Rachel made landfall. This second episode of heavy rainfall was also caused by the combined effects of orographic forcing and TS Rachel's rainbands, in which the strong orographic lifting of the LLJ triggered convective systems in the concave region of the southwest CMR. Based on the numerical results, the simulation of the large-scale environment of the two tropical storms helped the model to predict the location of the orographic precipitation. However, the observed precipitation over the western slope of the CMR could not be reasonably simulated, and the model slightly overestimated the total amount of precipitation. This discrepancy between observation and simulation could have been caused by the complex topography, which may not be able to be resolved in a 5-km-resolution grid-spacing domain, especially over the southwest CMR. This grid spacing results in about four grid points along the concave region. In addition, the model was not able to reproduce the intensity or convective structure of TS Rachel. Subsequently, the circulation of TS Rachel weakened as it came closer to southern Taiwan, which downplayed the impinging flow from the west. As a result, the precipitation over the western slope of the CMR could not be reasonably simulated. Even though TS Rachel is a weak tropical cyclone, it appears that vortex bogusing is needed at the initial stage in order to get a better result. On the other hand, the complex topography could play a role in disorganizing the subgrid-scale convection, resulting in the model overpredicting the total amount of precipitation. However, the model results provide good insight into the dynamics of moist convective systems over complex orography, and the periods of the orographic precipitation were predicted reasonably well.

The sensitivity simulation without orography helped to better gauge the role of the terrain during the heavy rainfall period. We found that the large-scale circulation had a greater contribution to the rainfall amounts and the distribution over southern Taiwan before Rachel made landfall. The heavy rainfall was closely related to the complex topography when TS Rachel moved inland, and the low-level impinging flow was dramatically changed by the slope as well as the concave area of southwestern Taiwan. We also examined the horizontal distribution of θ_e as well as the vertical cross sections of θ_e and q_c. The results indicate that high θ_e as well as unstable layers can be found on both the windward and lee sides of the topography; however, the heavy orographic rainfall existed only on the windward side (concave area). The results also suggest that southwesterly LLJ in association with high-θ_e airstream supplies moist air and helps establish the potentially unstable layer; combined with the orographic blocking effects as well as strong upward motion from TS Rachel, heavy orographic rainfall was produced.

By examining the orographically induced vertical moisture flux and general vertical moisture flux, we found that the rainfall distribution over the mountains

was roughly consistent with the orographically induced vertical moisture flux distribution. Hence, the orographic vertical moisture flux may serve as an index for predicting the potential threat area of upsloping heavy orographic rainfall, while the general vertical moisture flux could predict the rainfall distribution better over a flat surface. In addition, the mountain geometry (concave area) could help to enhance confluent flow and organize localized convective cells. Subsequently, outflow boundaries are produced by the convective cold pools, which force the convective systems to propagate upstream over the sea, and the impinging flow from the southwest develops new convection.

The results shown in this study are a first step toward better understanding of the factors necessary for producing heavy orographic rainfall, which may provide guidance for improving orographic rainfall forecasts. Although some other potential factors might still be embedded in orographic rainfall events, the results of this case study provided useful information. The high sensitivity of the orographic precipitation to the common ingredients found by Lin et al. (2001) and in this study suggests some subtle, sophisticated relationships between complex terrain and vertical moisture flux that require further study. More validation of modeling results against rainfall measurements is needed.

Acknowledgments. The authors would like to express their gratitude to the Naval Research Laboratory for their wonderful help with the COAMPS model. Discussions with Dr. S. Chang and Dr. M. L. Kaplan are highly appreciated. We also want to thank Drs. Ken Waight, Karl D. Pfeiffer, and Mr. James A. Thurman and Dr. R. P. Weglarz at Western Connecticut State University for proofreading the manuscript. Computations were performed at the North Carolina Supercomputing Center and the National Center for Atmospheric Research. Critical reviews of three anonymous reviewers have been very helpful. This research is supported by National Science Foundation Grant ATM-0096876.

REFERENCES

Alpert, P., 1986: Mesoscale indexing of the distribution of orographic precipitation over a high mountain. *J. Climate Appl. Meteor.*, **25,** 532–545.

Barker, E. H., 1992: Design of the navy's multivariate optimum interpolation analysis system. *Wea. Forecasting,* **7,** 220–231.

Buzzi, A., and L. Foschini, 2000: Mesoscale meteorological features associated with heavy precipitation in the southern Alpine region. *Meteor. Atmos. Phys.,* **72,** 131–146.

——, N. Tartaglione, and P. Malguzzi, 1998: Numerical simulations of the 1994 Piedmont flood: Role of orography and moist processes. *Mon. Wea. Rev.,* **126,** 2369–2383.

Cacciamani, C., D. Cesari, F. Grazzini, T. Paccagnella, and M. Pantone, 2000: Numerical simulation of intense precipitation events south of the Alps: Sensitivity to initial conditions and horizontal resolution. *Meteor. Atmos. Phys.,* **72,** 147–159.

Chang, S. W., 1983: A numerical study of the interaction between two tropical cyclones. *Mon. Wea. Rev.,* **111,** 1806–1817.

Chen, S.-H., and Y.-L. Lin, 2001: Orographic effects on a conditionally unstable flow over an idealized three-dimensional mesoscale mountain. *MAP Newsl.,* **15,** 246–249.

Chu, C.-M., and Y.-L. Lin, 2000: Effects of orography on the generation and propagation of mesoscale convective systems in a two-dimensional conditionally unstable flow. *J. Atmos. Sci.,* **57,** 3817–3837.

Davies, H. C., 1976: A lateral boundary formulation for multi-level prediction models. *Quart. J. Roy. Meteor. Soc.,* **102,** 405–418.

Dong, K., and C. J. Neumann, 1983: On the relative motion of binary tropical cyclones. *Mon. Wea. Rev.,* **111,** 945–953.

Doswell, C. A., III, H. Brooks, and R. Maddox, 1996: Flash flood forecasting: An ingredients-based methodology. *Wea. Forecasting,* **11,** 560–581.

——, C. Ramis, R. Romero, and S. Alonso, 1998: A diagnostic study of three heavy precipitation episodes in the western Mediterranean region. *Wea. Forecasting,* **13,** 102–124.

Durran, D. R., and J. B. Klemp, 1983: A compressible model for the simulation of moist mountain waves. *Mon. Wea. Rev.,* **111,** 2341–2361.

Fankhauser, J. C., 1988: Estimates of thunderstorm precipitation efficiency from field measurements in CCOPE. *Mon. Wea. Rev.,* **116,** 663–684.

Fujiwhara, S., 1921: The natural tendency towards symmetry of motion and its application as a principle in meteorology. *Quart. J. Roy. Meteor. Soc.,* **47,** 287–293.

Gal-Chen, T., and R. C. J. Somerville, 1975: On the use of a coordinate transformation to the solution of the Navier–Stokes equations. *J. Comput. Phys.,* **17,** 276–309.

Haack, T., 1996: Software user's manual—Coupled Ocean/Atmosphere Mesoscale Prediction System. NRL Memo. Rep. 7227, 76 pp.

Harrold, T., 1973: Mechanisms influencing the distribution of precipitation within baroclinic disturbances. *Quart. J. Roy. Meteor. Soc.,* **99,** 232–251.

Harshvardhan, R. Davies, D. Randall, and T. Corsetti, 1987: A fast radiation parameterization for atmospheric circulation models. *J. Geophys. Res.,* **92,** 1009–1015.

Hodur, R. M., 1997: The Naval Research Laboratory's Coupled Ocean/Atmosphere Mesoscale Prediction System (COAMPS). *Mon. Wea. Rev.,* **125,** 1414–1430.

Hogan, T. F., T. E. Rosmond, and R. Gelaro, 1991: The NOGAPS forecast model: A technical description. Naval Oceanographic and Atmospheric Research Laboratory Rep. 13, 220 pp. [Available from Naval Research Laboratory, Monterey, CA 93943-5502.]

Kain, J. S., and J. M. Fritsch, 1993: Convective parameterization for mesoscale models: The Kain–Fritsch scheme. *The Representation of Cumulus Convection in Numerical Models, Meteor. Monogr.,* No. 46, Amer. Meteor. Soc., 165–170.

——, and ——, 1998: Multiscale convection overturning in mesoscale convective systems: Reconciling observations, simulations, and theory. *Mon. Wea. Rev.,* **126,** 2254–2273.

Klemp, J. B., and R. Wilhelmson, 1978: The simulation of three-dimensional convective storm dynamics. *J. Atmos. Sci.,* **35,** 1070–1096.

Lander, M. A., 1995: The merger of two tropical cyclones. *Mon. Wea. Rev.,* **123,** 2260–2272.

Lin, Y.-L., 1993: Orographic effects on airflow and mesoscale weather systems over Taiwan. *Terr. Oceanic Atmos.,* **4,** 381–420.

——, R. D. Farley, and H. D. Orville, 1983: Bulk parameterization of the snow field in a cloud model. *J. Climate Appl. Meteor.,* **22,** 40–63.

——, S. Chiao, T.-A. Wang, M. L. Kaplan, and R. P. Weglarz, 2001: Some common ingredients for orographic flooding and heavy rainfall. *Wea. Forecasting,* **16,** 633–660.

Louis, J. F., 1979: A parametric model of vertical eddy fluxes in the atmosphere. *Bound.-Layer Meteor.,* **17,** 187–202.

Maddox, R. A., 1983: Large-scale meteorological conditions associated with midlatitude mesoscale convective complexes. *Mon. Wea. Rev.,* **111,** 1475–1493.

Romero, R., C. A. Doswell III, and C. Ramis, 2000: Mesoscale numerical study of two cases of long-lived quasi-stationary convective systems over eastern Spain. *Mon. Wea. Rev.,* **128,** 3731–3751.

Rutledge, S. A., and P. V. Hobbs, 1983: The mesoscale and microscale structure of organization of clouds and precipitation in midlatitude cyclones. VIII: A model for the ''seeder-feeder'' process in warm-frontal rainbands. *J. Atmos. Sci.,* **40,** 1185–1206.

Schneidereit, M., and C. Schär, 2000: Idealized numerical experiments of Alpine flow regimes and southside precipitation events. *Meteor. Atmos. Phys.,* **72,** 233–250.

Sinclair, M. R., 1994: A diagnostic model for estimating orographic precipitation. *J. Appl. Meteor.,* **33,** 1163–1175.

Therry, G., and T. Lacarrére, 1983: Improving the eddy kinetic energy model for planetary boundary layer description. *Bound.-Layer Meteor.,* **25,** 63–88.

Wu, C.-C., and Y.-H. Kuo, 1999: Typhoons affecting Taiwan: Current understanding and future challenges. *Bull. Amer. Meteor. Soc.,* **80,** 67–80.